Lasers in Manufacturing Conference 2019

Quantitative Analysis of the Temporal Distance between Melt Waves on the Cutting Front Apex during Laser Fusion Cutting of Stainless-Steel Sheet Metal with 1 Micron Wavelength

D. Arntz[a,*], D. Petring[b], F. Schneider[b], S. Stoyanov[b], U. Halm[c], A. Gillner[a,b]

[a]*RWTH Aachen University, Chair for Laser Technology LLT, Steinbachstr. 15, 52074 Aachen, Germany*
[b]*Fraunhofer Institute for Laser Technology ILT, Steinbachstr. 15, 52074 Aachen, Germany*
[c]*RWTH Aachen University, Nonlinear Dynamics of Laser Processing NLD, Steinbachstr. 15, Aachen, 52074, Germany*

Abstract

Instabilities of the melt flow dynamics on the laser cutting front cause loss of quality due to the formation of striations on the cut flank. Only individual aspects of mechanisms of striation generation during laser cutting are understood. Further evaluations of the melt flow dynamics inside laser cutting kerfs regarding characteristic temporal and spatial variables of the cutting process and their dependences are still necessary. Within this paper the melt flow dynamics during laser cutting of 6 mm thick stainless steel using a disk laser with a laser power of 5 kW are visualized and analyzed by means of in-situ high-speed video diagnostics (>100,000 fps). For that purpose, an advanced algorithm is used to detect the temporally and spatially resolved melt waves sliding down along the cutting front apex. The cutting depth-dependent analysis of the temporal distance between the melt waves reveals only a low dependence on the cutting velocity.

Keywords: Macro Processing; Cutting; 1 micron laser; high-speed imaging; melt flow; process diagnostics

1. Introduction

High-performance laser cutting systems for macro processing are mainly equipped with CO_2 and fiber or disk lasers. The achievable cutting quality is constantly being improved, but the achievable cutting quality in thick sheet cutting with fiber or disk lasers is still significantly lower than with CO_2 lasers.

* Corresponding author.
E-mail address: dennis.arntz@llt.rwth-aachen.de .

Instabilities of the laser cutting front lead to quality losses in the form of striations on the resulting cut flank and can even lead to burr formation. Only individual aspects of mechanisms of striation generation during laser cutting are understood. In recent years, Hirano and Fabbro, 2011 , Ermolaev et al., 2014 and Pocorni et al., 2015 have pushed important work on in-situ high-speed visualization of the melting and solidification dynamics during the cutting process. Hirano and Fabbro were able to observe the formation of melting plateaus, which they describe as "humps", in the upper area of wide kerfs (width >1.7 mm) at low assist gas pressures (p=2.5 bar). They used 3 mm thick stainless-steel samples and determined a melt flow velocity of about 3.2 m/s and a hump velocity of 0.2 m/s. Ermolaev et al. reported for 6 mm thick stainless-steel samples, velocities of melt ejections along narrow tracks of up to 10 m/s. Pocorni et al. describe velocities of melt accumulations, which they called “bumps”, with an average velocity of ≈0.4 m/s and an average melt flow velocity of ≈1.1 m/s for 10 mm thick stainless-steel samples. By using in-situ high-speed recordings and an advanced algorithm (Arntz et al., 2019) we were able to evaluate quantitatively the melt flow dynamics and velocity distribution of melt waves on the cutting front apex. With this method it could be shown that a dominant amount of the melt waves reaches velocities of 15 m/s. It could be shown that a stable melt film and fast melt waves are beneficial to achieve a good cut flank quality.

Beside this, further evaluations regarding characteristic temporal and spatial variables of the cutting process and their dependences are necessary. The main objective of this work is to investigate and correlate the temporally and spatially resolved melt waves sliding down along the cutting front apex with the striation pattern on the resulting cut flank for different cutting velocities.

2. Experimental Setup

2.1. Process parameters and in situ diagnostic procedure

The experiments were carried out using a 12 kW disk laser (Trumpf, TruDisk 12002) with a wavelength of 1030 nm at an output power of 5 kW. A Precitec HP SSL cutting head was used and the fiber (Ø 200 µm) guided laser beam was collimated and focused with focal lengths of 100 mm and 250 mm, respectively. This configuration provides a focal diameter of 500 µm. A conical-cylindrical nozzle with a diameter of 5 mm was mounted and a stand-off distance of 0.7 mm was adjusted. To cut 6 mm thick stainless-steel samples a focus position 4 mm below the upper surface of the sample and an assist gas pressure of 20 bar in combination with four different cutting velocities (v_c: 0.8; 1.8; 2.8; 3.8 m/min) were used.

In order to visualize and analyze the melt flow dynamics at the cutting front apex, incisions were made, and the direction of observation was aligned through the evolving cut kerf (Fig. 1; a). The region of interest of the used high-speed camera (Photron SA 5) was set to 64 x 376 px, to facilitate a recording frame rate of 140,000 fps. By using a NIKON 200 mm macro lens a spatial resolution of 20 µm/px was enabled. To eliminate artifacts from the start of the cut and to ensure a sufficient statistical evaluation of the velocity distribution, the evaluation start was placed 2 mm behind the start of the cut and for each evaluation a cutting section of 5 mm was used. (Fig. 1; a)

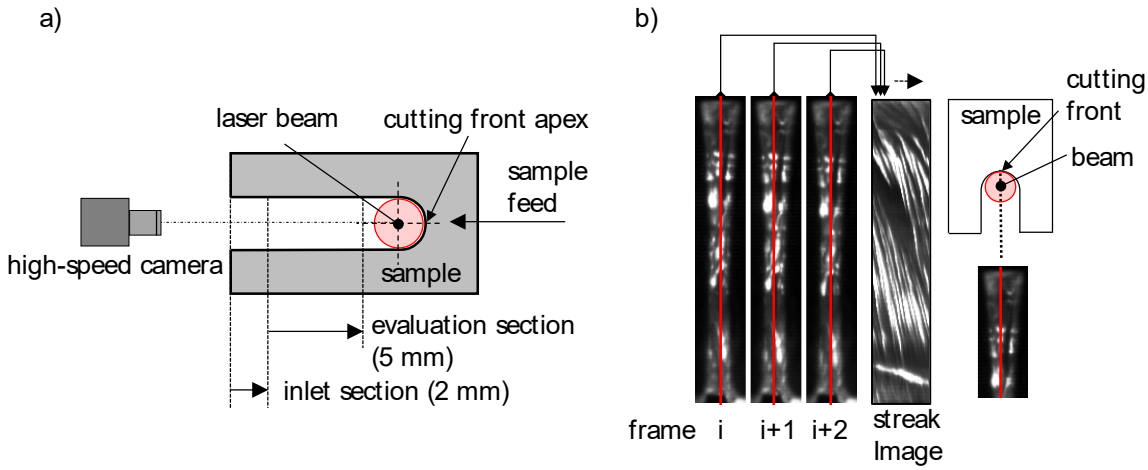

Fig. 1. (a) Principle of in-situ diagnosis setup for incisions; (b) Principle of streak image procedure

2.2. Algorithm for evaluating the melt flow dynamics

To evaluate the melt flow dynamics, an algorithm was developed to detect the occurring brightly shining melt waves on the cutting front out of the high-speed video-recordings. To achieve this, a Peak-Finder programmed by Bergman S., 2019 was adapted to analyze the horizontal (temporal) distribution of the gray-scale values from streak images (Fig. 1; b) in each cutting depth. To do this, horizontal analysis bars were placed in each single horizontal pixel line of the streak image (Fig. 2).

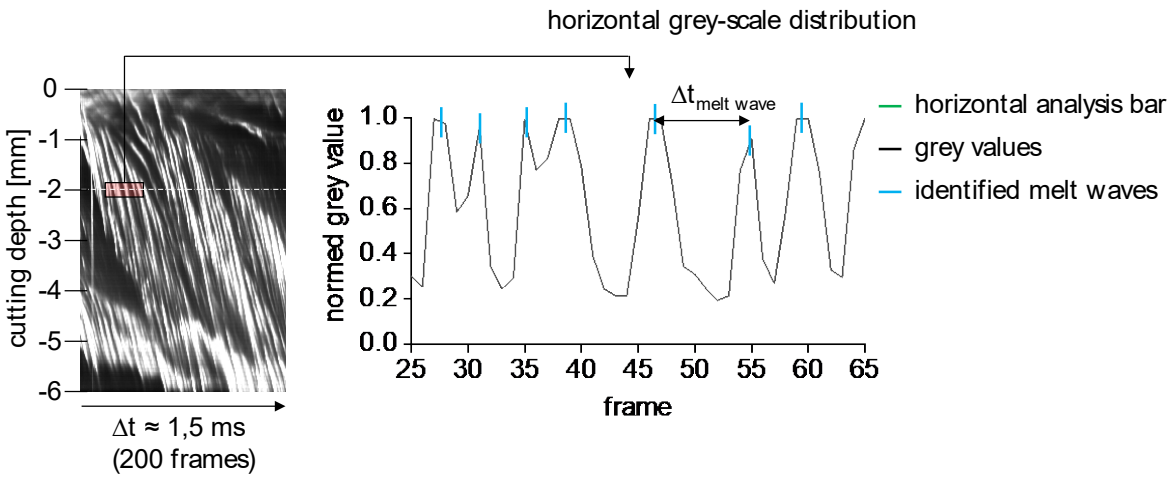

Fig. 2. Principle of cutting depth-dependent melt wave identification procedure for a cutting depth of 2 mm and a selection of 40 frames

The peaks and thus the melt waves were assigned to the temporal process progress and the cutting depth. To consider different lengths of process durations due to the different cutting velocities, the number

of melt waves were normalized over time. By knowing the time-dependent location of each melting wave, a cutting depth-dependent analysis of the temporal distance between the melt waves becomes possible (cf. Fig. 4).

3. Results & Discussion

In the following section, the average surface roughness of cut flanks (Fig. 3) and the results of the in-situ diagnosis of incisions are quantitatively analyzed and discussed for different cutting velocities (Fig. 4).

3.1. Characterization of cut flanks

An increase of the cutting velocity (v_c) while maintaining focus position and assist gas pressure leads to an overall reduction in the surface roughness, whereby the reduction varies greatly versus cutting depth (Fig. 3). In a cutting depth of -0.5 mm, the surface roughness decreases with increasing cutting velocity from R_z≈55 µm for v_c=0.8 m/min to R_z≈30 µm for v_c=3.8 m/min. The lowest average surface roughness (R_z≈ 20 µm) and the lowest dependence on cutting velocity is achieved around a cutting depth of -2 mm. At larger cutting depths, the average surface roughness increases for all four examined cutting velocities. The average surface roughness for v_c=3.8 m/min is still the lowest (R_z≈25 µm), the average surface roughness for v_c=2.8 m/min increases to R_z≈30 µm and surface roughness of R_z≈55 µm occurs for v_c=0.8 m/min and v_c=1.8 m/min. In summary, the course of the surface roughness over cutting-depth is more or less S-shaped.
(Fig. 3)

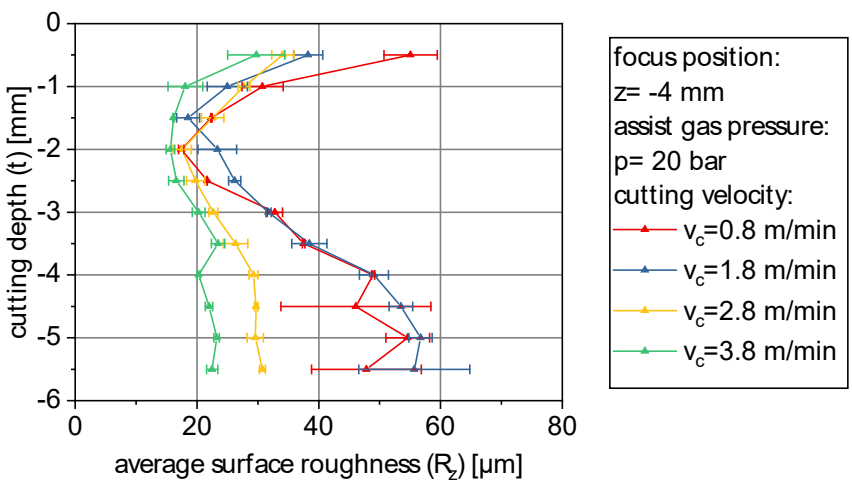

Fig. 3. Average surface roughness measurements for different cutting velocities a focus position of z=-4 mm and an assist gas pressure of p=20 bar

3.2. Temporal distance between melt waves

In order to discuss the temporal distance of the melt waves sliding downwards at the cutting front apex, the frequencies of occurrence over different cutting depths are plotted (Fig. 4). The minimum captured time interval between two separate melt waves is 15 µs, which corresponds to two frames. This time difference results from the recording framerate of 140,000 fps. In addition to the distribution, the cutting depth-

dependent modal value, the lower and upper quartile and the global maximum frequency are marked. (Fig. 4)

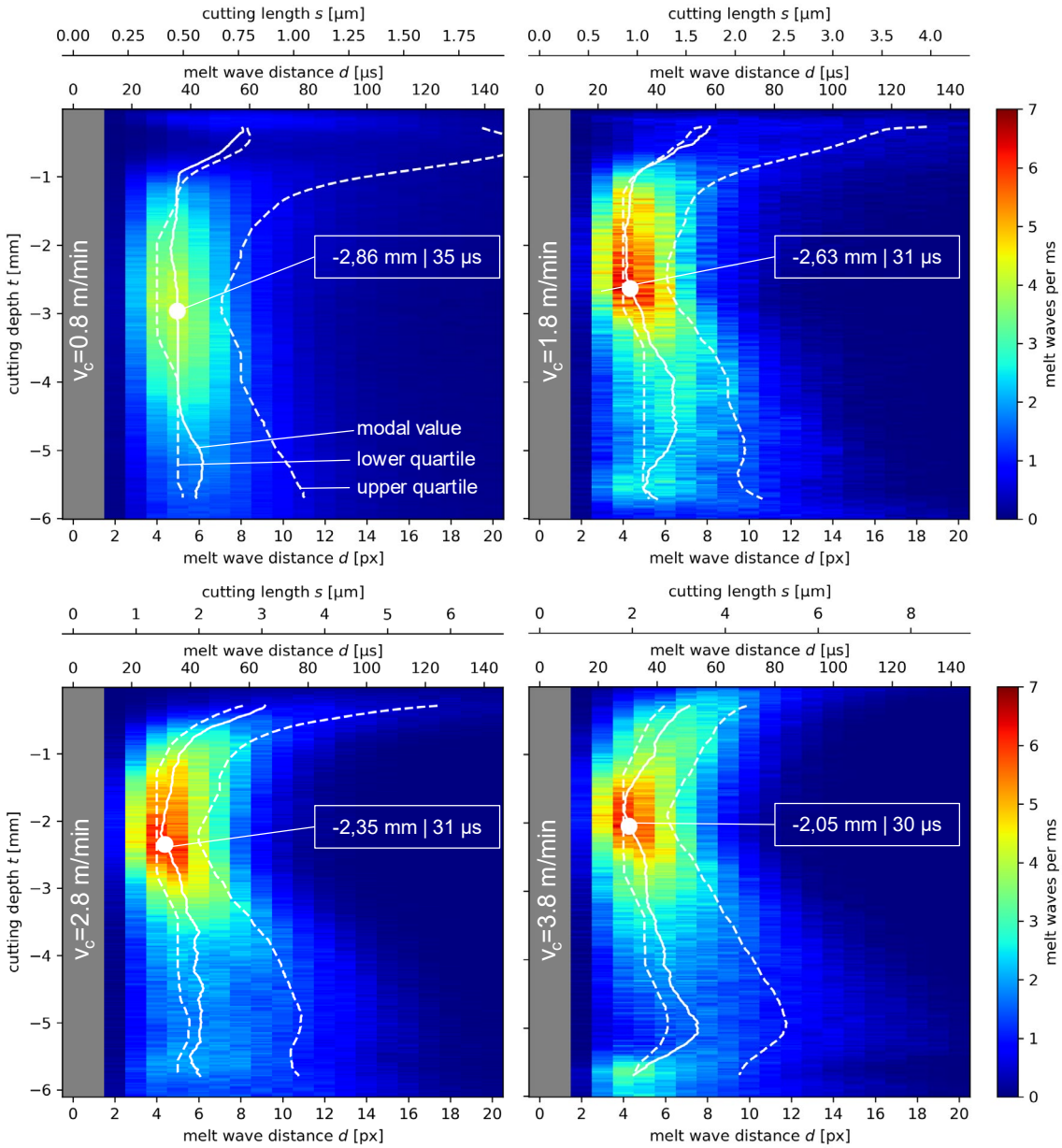

Fig. 4. Cutting depth-dependent analysis of the temporal distance between melt waves for different cutting velocities. From top left to bottom right: v_c: 0.8; 1.8; 2.8 and 3.8 m/min

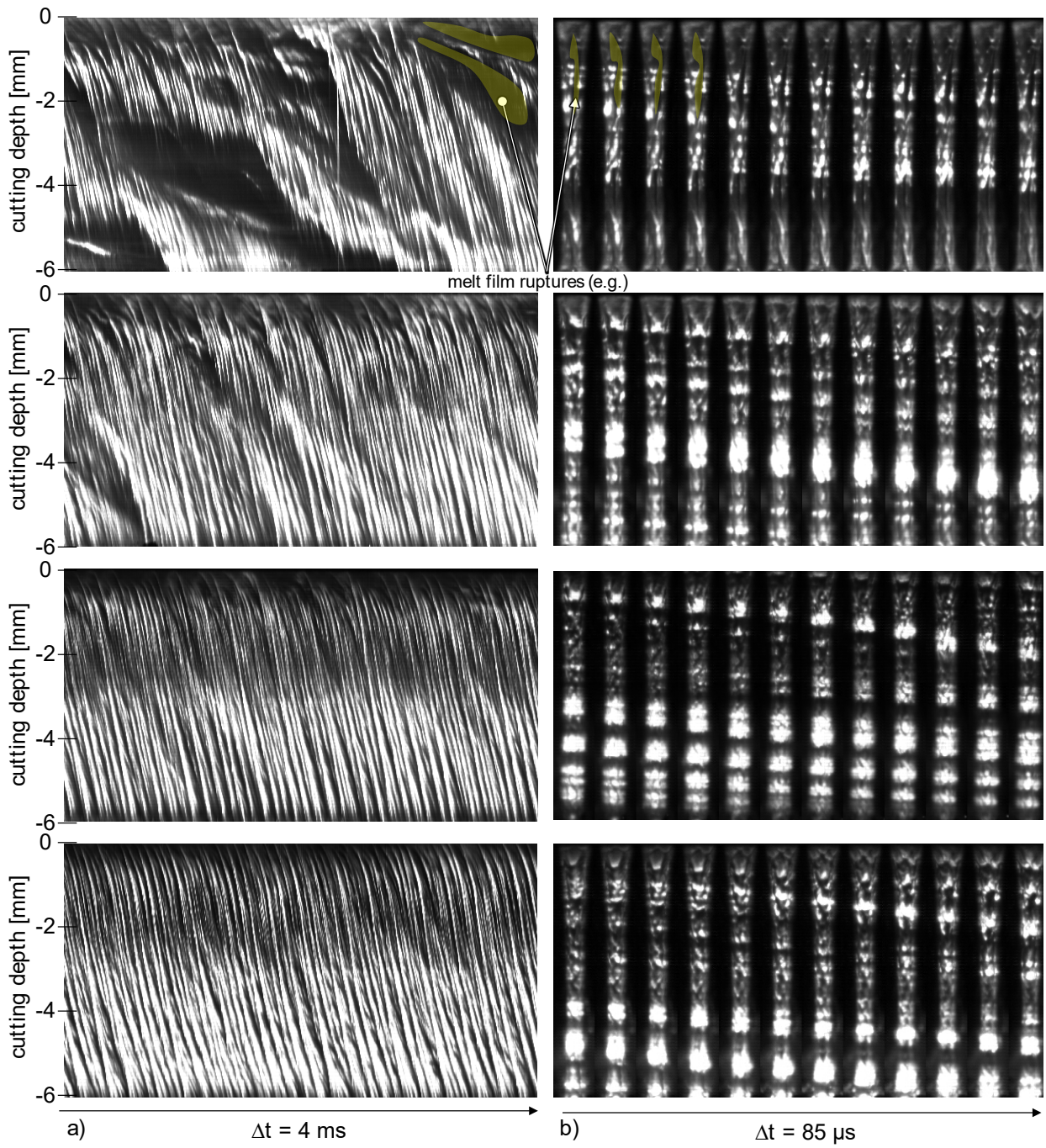

Fig. 5. Extraction of streak images (a) and frame by frame analysis (b) of in-situ high speed video diagnostics for different cutting velocities. Top to bottom: v_c: 0.8; 1.8; 2.8 and 3.8 m/min

For the four investigated cutting velocities, characteristic frequency distributions of the cutting depth-dependent time distance of the melt waves can be identified (Fig 4). The modal values (Fig. 4; white line) plotted over the cutting depth show a more or less S-shaped course from the top to the bottom of the sheet. In this case, the pronunciation of the S-form increases with increasing cutting velocity. This is in contrast to the roughness depth, where a decrease in the pronunciation of the S-shape can be observed (Fig. 3).

From the kerf entry to a cutting depth of -1 mm, the modal value of the temporal melt wave distance is reduced from ≈60 µs to ≈40 µs. In the more progressed cutting depth range (-1 mm to -3 mm) the modal value is reduced to 30-35 µs. For the cutting velocities of 1.8, 2.8 and 3.8 m/min, the modal value shows a quantitatively similar number of melt waves per time (up to 7 melt waves per millisecond) with almost the same time interval (≈30 µs). At the lowest cutting velocity, the number of melt waves is lower (up to 4 melt waves per millisecond), whereby the time interval of the melt waves is slightly increased to 35 µs. For the lowest cutting velocity the global maximum value can be identified in a cutting depth of -2.9 mm. With increasing cutting velocity, the global maximum value is shifted to smaller cutting depths (-2.6 mm to -2.0 mm). The vertical expansion of the maximum regime is reduced. The upper range of the vertical expansion of the maximum regime is nearly unchanged. At the same time, the increase in cutting velocity leads to an increase in the amount of melt waves at a very small cutting depth (above -0.5 mm) The cutting depth dependent analysis of the temporal distance of the melt waves (Fig. 4) shows in this area that the modal value for the highest investigated cutting velocity consists of more melt waves than for the lower cutting velocities. As the cutting velocity is reduced, the start of this region, where more than at least two melt waves per millisecond are detected, shifts in the direction to larger cutting depths. With a further increase in the cutting depth (-4 mm to -5 mm), the modal values of the frequency distributions are in the range of 40-50 µs, whereby the distribution is wider overall and increases with an increase in the cutting velocity. (Fig. 4)

The streak images generated from the video data (Fig. 5) and used for the above image processing represent an instructive view of the melt film dynamics on the cutting front apex. They show a more homogeneous image with increasing cutting velocity. Melt waves (bright lines in the streak images) become more regular both horizontally (temporally) and vertically (locally). With increasing cutting depth (until ≈-2 mm) the velocity of the melt waves increases, and the formation of additional individual melt waves of nearly the same velocity can be observed. The time interval between the melting waves is reduced. This differs from larger cutting depth (below ≈-3 mm). In larger cutting depth, additional melt waves are formed, whereby the melt wave velocity is partially reduced. The corresponding single image sequences (Fig. 5 b) show that a horizontal separation of already formed melt waves occurs in this area. This effect leads to an increase of the distribution width in the larger cutting depth range. Thus, the formation of at least two horizontal areas, comparable to the temporal melt wave distribution until and below a cutting depth of ≈-2 mm, can be identified. Distinct regions can also be taken from the roughness depth measurements, whereby the roughness depth is lowest near to the horizontal transition area. In addition, the melt wave distribution shows the global maximum with the smallest time intervals in this transition area.

The width of the distribution correlates with the regularity of the melt wave dynamics (compare Fig. 4 with Fig. 5). Until a cutting depth of ≈-2 mm, the increase in the regularity of the melting waves correlates positively with a reduction of the surface roughness. The wider distribution width in smaller cutting depths at lower cutting velocities is the result of irregular melt wave dynamics, which can be characterized by melt string formations or melt film ruptures (Fig. 5). For larger cutting depths (below ≈-2 mm) the correlation between the regularity of the melt wave dynamics and the surface roughness is negative. Although the distribution width is the widest for the highest cutting velocity, the surface roughness in this area is the lowest. One reason for this may be the examination of only a small central vertical area near the cutting

front apex. This procedure allows the analysis of individual waves. However, it compromises the analysis because the transition of the melt film to the cutting flank cannot be analyzed in this manner.

It can be shown that from a cutting depth of ≈-2 mm multiple reflections in the cut kerf have a considerable influence on the formation of the lateral cutting flanks (Petring et al., 2012; Arntz et al., 2018). The reflections are partly generated at small cutting depths whereby the cutting flank is affected at larger cutting depths. Even regular melt wave dynamics on the cutting front apex at small cutting depths can thus lead to a more homogeneous illumination at larger cutting depth due to regular multiple reflections. On the other hand melt film strings or melt film ruptures which are formed at small cutting depths, lead to an increased average surface roughness not only in small cutting depths but also in larger cutting depths.

The results allow the assumption that regular melt wave formations on the cutting front apex at small cutting depths are the basis for a low cut flank roughness of the complete cut flank. Since the smallest temporal melt wave distance and the smallest surface roughness of the cut flank can be determined in a cutting depth of approximately ≈-2 mm, a small temporal melt wave distance seems to be beneficial for a reduction of the surface roughness.

Interesting is the aspect that the cutting depth-dependent analysis of the temporal distance between the melt waves reveals only a low dependence from the cutting velocity. This aspect allows the assumption that the time interval of the melt waves between 30-35 µs is characteristic for the investigated process parameter field. An explanation for this behavior will be published elsewhere.

4. Conclusion & Outlook

The presented approach for the analysis of the temporal and local melt wave distribution on the cutting front apex by quantitative evaluation of streak images allows the following statements:

- The basis for a cut flank with a low average surface roughness is a stable melt film that permanently wets the cutting front.
- Regular melt wave formations on the cutting front apex at small cutting depths are beneficial for a low cut flank roughness of the complete cut flank.
- The regularity of the melt wave frequency can be achieved at smaller cutting depths with higher cutting velocities.
- A small temporal melt wave distance seems to be beneficial for a reduction of the surface roughness.
- In the investigated cutting velocity range (v_c: 0.8 - 3.8 m/min) a characteristic time of 30-35 µs can be found for the temporal melt wave distance.

The results are a basis for the development of optimization strategies for the reduction of the cut flank roughness depth. In future work an even higher temporal resolution of the in-situ diagnosis should be applied to validate the lower limit of the temporal melt wave distance. Further parameter variations, such as variation of the assist gas pressure or the focus position, should be evaluated.

Acknowledgements

The presented investigations were carried out at the Chair of Laser Technology LLT of RWTH Aachen University and Fraunhofer Institute for Laser Technology ILT within the framework of the Collaborative Research Centre SFB1120-236616214 “Bauteilpräzision durch Beherrschung von Schmelze und Erstarrung in Produktionsprozessen” and funded by the Deutsche Forschungsgemeinschaft e.V. (DFG, German Research Foundation). The sponsorship and support is gratefully acknowledged.

References

Arntz, D., Petring, D., Stoyanov, S., Jansen, U., Schneider, F., Poprawe, R., 2018. “In situ visualization of multiple reflections on the cut flank during laser cutting with 1 µm wavelength,” in Journal of Laser Applications 30, 032206 (2018); DOI: 10.2351/1.5040614.

Arntz, D., Petring, D., Schneider, F., and Poprawe, R., 2019. “In situ high speed diagnosis—A quantitative analysis of melt flow dynamics inside cutting kerfs during laser fusion cutting with 1 µm wavelength,” in Journal of Laser Applications 31, 022206 (2019); DOI: 10.2351/1.5096091.

Bergman, S., 2019. “Peak detection in Python,” see https://gist.github.com/sixtenbe/1178136 (accessed 19 April 2019).

Ermolaev, G. V., Yudin, P. V., Briand, F., Zaitsev, A. V. and Kovalev, O. B., 2014. “Fundamental study of CO2- and fiber laser cutting of steel plates with high speed visualization technique,” J. Laser Appl. 26, 42004 (2014); DOI: 10.2351/1.4895563.

Hirano, K., Fabbro, R., 2011. “Experimental investigation of hydrodynamics of melt layer during laser cutting of steel,” J. Phys. D Appl. Phys. Vol. 44, 105502 (2011); DOI: 10.1088/0022-3727/44/10/105502.

Petring, D., Molitor, T., Schneider, F., and Wolf, N., 2012. “Diagnostics, modeling and simulation: Three keys towards mastering the cutting process with fiber, disk and diode lasers. Procedia 39, 186–196 (2012); DOI: 10.1016/j.phpro.2012.10.029.

Pocorni, J., Petring, D., Powell, J., Deichsel, E. and Kaplan, A. F. H., 2015. “Measuring the melt flow on the laser cut front,” Phys. Proc. 78, 99–109 (2015); DOI: 10.1016/j.phpro.2015.11.022.